

## Wide Color Gamut Five Channel Multi-Primary Display for HDTV Application

Moon-Cheol Kim, Yoon-Cheol Shin and Jin-Sub Um

Digital Media R&D Center, Samsung Electronics Co. Ltd., Suwon City, Gyeonggi-Do, REP. OF KOREA

Wide color gamut displays using monochromatic light sources, such as LED or laser, or applying multi-primary techniques have been introduced by several authors in forms of laboratory based models and for high end natural color vision applications. In order to bring these technologies into the consumer market, one of our latest investigations resulted in a rear projection type high definition multi-primary display (MPD) system which has been realized by a modification of our previous three channel DLP™ projection television. Thereby the full spectral energy of the UHP™ type projection lamp is sequentially separated into five primary spectrums through a rotating color wheel instead of the conventional RGB primary colors so that it enables to reproduce a wide range of colors than sRGB compatible display. The main focus of this study is to describe a gamut mapping method that allows using a full range of color gamut of MPD for a given limited color gamut of television signal. This approach is to display an image in such a way that the limited color saturations of the current television signal are adaptively enhanced for every observer. Through the gamut mapping, the picture quality of MPD is significantly improved in comparison with a conventional display system.

Journal of Imaging Science and Technology 46: 594–604 (2005)

### Introduction

Historically, the color gamut of HDTV standard (ITU R. BT. 709) covers approximately 76% of all reflected colors of natural objects.<sup>1</sup> Therefore, some highly saturated colors can not be reproduced on such display systems. In other words, all colors of outside the Rec. 709 color gamut can be clipped on the boundary of the Rec. 709 gamut by signal processing in conventional camera systems, or by an appropriate gamut mapping algorithm in even more sophisticated cameras. Hence, we can only see similar colors within the display color gamut instead of very highly saturated original colors. This clipping may finally result in a desaturation of those colors.

Furthermore, we now can see many more artificial colors with higher saturation, such as colors of pigments, paints, clothing materials and monochromatic illuminant colors in our modern life. Because of the increased population of such highly saturated colors, a wide color gamut imaging system will be needed. Therefore, the International Telecommunication Union (ITU) and International Electro-Technical Committee (IEC) already published the wide color gamut signal definitions of ITU-R.BT.1361 and extended sRGB.<sup>2,3</sup>

In recent imaging technology, several authors introduced multispectral imaging systems to capture and reproduce a wide range of colors. Especially in the display field, wide gamut displays using pure color light

sources with narrow spectral radiance, such as RGB-lasers<sup>4,5</sup> and high power LEDs,<sup>6</sup> or applying multi-primary techniques have been introduced.<sup>7–12</sup>

Among these, the multi-primary display technique can be easily realized for a projection type display system with minimum cost. For an application of this technology, our latest investigation resulted in a five primary MPD. Thereby, the prototype MPD has been realized by a color wheel modification of our previous RGB DLP™ projection television with 50/60" screen size. To get the primary colors, the full spectral energy of a 120W UHP™ projection lamp is sequentially separated into five primary spectral bands through a rotating color wheel with five interference filter segments. Figure 1(a) shows the relative spectral irradiances of the primary colors, and their chromaticity coordinates on CIE-UCS color chart (Fig. 1(b)) in comparison with the gamut of Rec. 709 (sRGB).

The gamut volume comparison of displays with different number of primary colors on such two dimensional color space (Fig. 1(b)) is unsuitable because of the lack of luminance information. For that reason, the gamut volume of the MPD can be examined in a uniform three-dimensional color space. Based on CIE-L\*a\*b\* color space (Fig. 2(a)), the color gamut volume of the MPD is approximately 1.5 times larger than Rec. 709. (It will be explained more precisely below.) Hence, the multi primary HDTV system is able to reproduce not only the limited colors of Rec. 709 but also some extended colors.

Even though the wide gamut signal has been defined, there are yet no available wide gamut signals or video streams in the broadcasting network. To utilize the full range of color gamut of MPD for the given limited Rec. 709 signal, a gamut matching method has been developed and applied between two color gamuts.

Original manuscript received July 22, 2004

Corresponding Author: M.-C. Kim, mc.kim@samsung.com

©2005, IS&T—The Society for Imaging Science and Technology

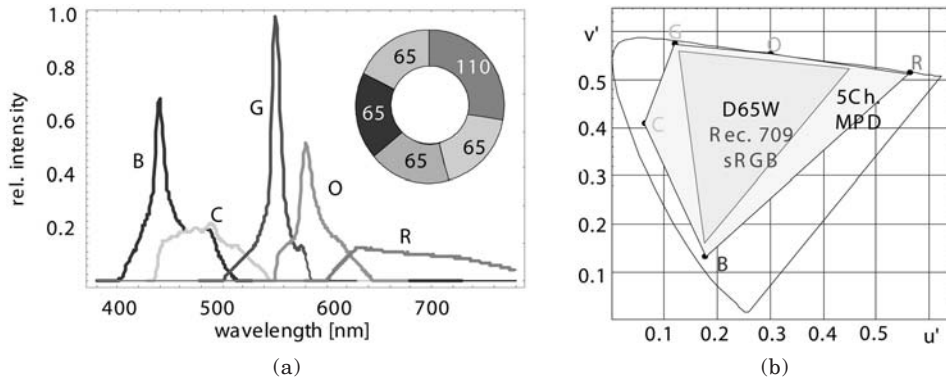


**Figure 1.** (a) Relative spectral irradiances of primary colors and the color wheel configuration (inside numbers indicate the occupation angle of each filter segment), and (b) primary color coordinates on CIE- $u'v'$  color chart.

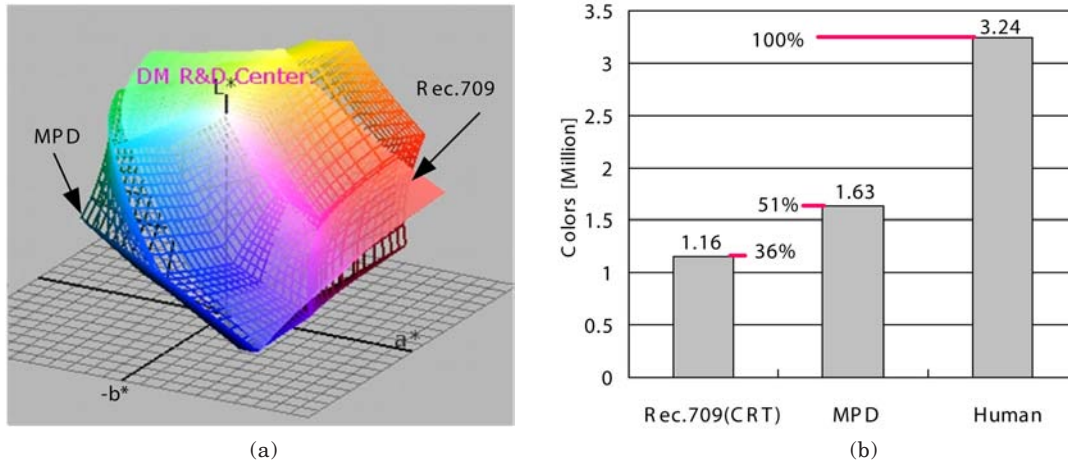


**Figure 2.** (a) Perspective view of the MPD gamut in CIELAB<sub>76</sub> color space in comparison with the Rec.709 (sRGB) gamut, and (b) gamut volume comparison: distinguishable colors of CRT, MPD and Optimal Color Space(human) for CIE 2° standard observer.

### Color Gamut

The realized MPD system has five primary colors of Red, Green, Blue, and additional Cyan and Orange color primaries which are optimally chosen for the given spectral characteristics of the UHP lamp, for the transmittance characteristics of the additional projection optics, and for the D65 display white. Because of the linear characteristic of DMD™ (digital mirror device) and faithful digital electronic circuits, the conventional additive display model suits very well for the MPD system. With a negligible black offset the forward model can be described as  $\mathbf{F} = \mathbf{M} \cdot \mathbf{C}$ , with the tristimulus color vector  $\mathbf{F} = (X, Y, Z)^T$  and linear display control vector

$$\mathbf{C} = (C_1, C_2, C_3, C_4, C_5)^T. \quad (1)$$

Thereby, the conversion matrix  $\mathbf{M}$  is obtained from the measurement of tristimulus values of the 5 primary colors using a spectroradiometer (Minolta CS1000).

$$\mathbf{M} = \begin{pmatrix} X_1 & X_2 & X_3 & X_4 & X_5 \\ Y_1 & Y_2 & Y_3 & Y_4 & Y_5 \\ Z_1 & Z_2 & Z_3 & Z_4 & Z_5 \end{pmatrix} \quad (2)$$

With the model equation, the gamut volume of MPD can be calculated for given control vectors on the gamut boundary and converted these values into CIELAB<sub>76</sub> uniform color space. In the uniform space, we calculated and compared volume sizes of the three different color gamuts of Rec. 709, MPD and an Optimal Color Space according to the computational method of Hill.<sup>13</sup> Accordingly, the optimal color space represents all human visible colors for the CIE 2° standard observer.

For this computation, we took unit spheres with diameter of  $\Delta E_{ab} = 1$  (as a just noticeable difference) and completely filled up each color gamut with those spheres. Then, we counted all the spheres inside the gamut volume. The total number of spheres is shown in Fig. 2(b). It reflects the total number of distinguishable colors for human eye based on CIELAB<sub>79</sub> color space. As shown in Fig. 2(b), the MPD has about 1.5 times more than Rec. 709(CRT) gamut and covers approximately 51% of the optimal color space.

Even though the MPD has larger volume of the color gamut than Rec. 709, in some color regions Rec. 709 has larger chroma values as shown in Fig. 2(a). Because, in MPD, the common reference white is composed of the five time-sequential primary colors instead of three primaries, the luminance level of each RGB primaries of

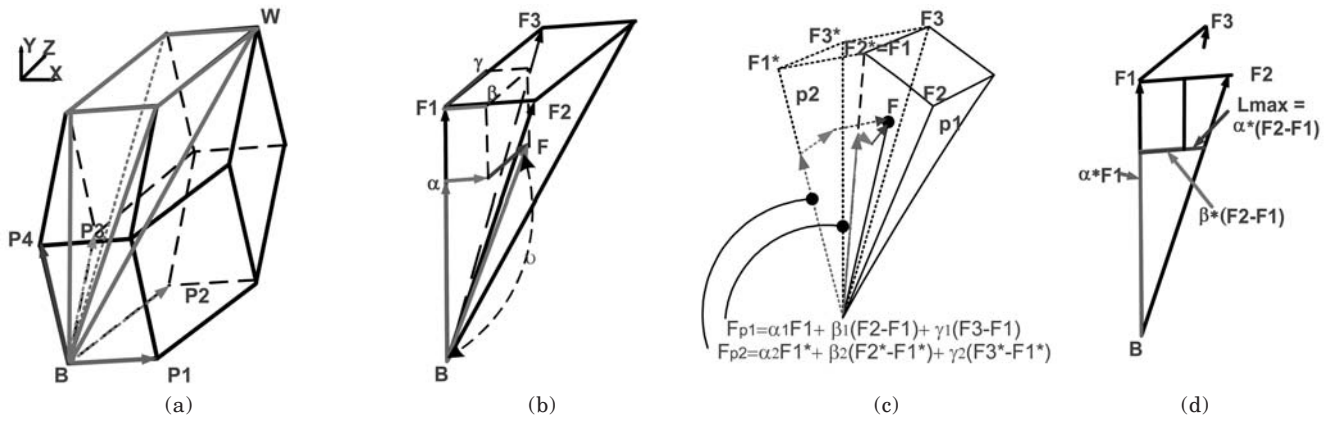


**Figure 3.** (a) Color gamut in XYZ space, (b) vector addition within the pyramid, (c) case of multiple solution, and (d) illustration for constraint check.

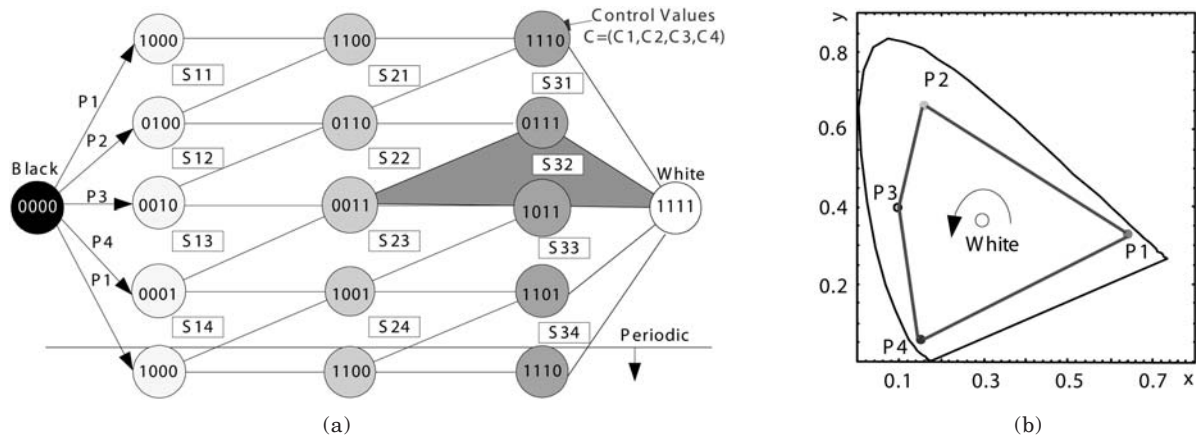


**Figure 4.** (a) Graphical gamut surface analysis, and (b) chromaticity diagram for an example display with 4 primaries.

MPD is therefore lower than the three-channel system (Rec.709).

### Inverse Display Model

Because of the non-square matrix  $M$  of Eq. (1), the matrix inversion is not unique for the CIE-XYZ tristimulus reproduction due to the violation of the physical constraint of the control vector. To solve this problem, several methods have been published.<sup>7,9-11</sup> What we utilized is the modified matrix switching of Ajito.<sup>10</sup> In this method, the MPD gamut splits into a certain number of pyramids. Then, the control vector is calculated by solving the linear equations for given XYZ triplet within a given pyramid. Accordingly, a pyramid needs to be selected in which a given tristimulus vector is included.

To find this pyramid, the two-dimensional chromaticity-LUT with corresponding pyramid numbers for input chromaticity values in  $xy$  or  $u'v'$  had been used. Normally, this method requires large amount of LUT-memories for the proper searching of pyramids on the boundaries of adjacent pyramids, typically over 1000 × 1000 address range.<sup>10</sup>

Our modified method tries to obriate such additional LUTs. Instead, we apply parallel processing for candidate pyramids and an appropriate algorithm decides a possible solution by checking the constraint conditions afterwards.

Figure 3(a) shows an example of a color gamut with four primaries ( $P = 4$ ) in XYZ color space. The color gamut can be then split into  $P(P - 2)$  pyramids without overlapping. The pyramid has 5 vertices including one common vertex as the black point of the XYZ color gamut.

To get all the vertex information on the pyramids, a simple graphical analysis of the gamut surface has been newly developed as shown in Fig. 4(a). This assumption is only valid if all the primary colors are located on a surface of the color gamut. Normally, all vertices on the gamut surface have the extreme control values of zero or one in normalized control value form, as indicated by a circular node (Fig. 4(a)).

Now, we can construct the diagram from black point “0000” to white “1111” with an incremental setting of channel control values, as shown in Fig. 4(a). For example, the first step is to assign  $P1$ – $P4$  primary colors (nodes 1000, 0100, 0010, 0001) in counterclockwise direction as shown in Fig. 4(b). In the second step, other surface vertices (1100, 0110, and so on) are constructed by the two neighboring vertices of the nodes from the first step. In this manner, the diagram should be completed until the white point is assigned as (1111). From this diagram of the gamut surface, we get the generalized information that the MPD with  $P$  primaries has  $P(P - 1) + 2$  number of surface vertices and  $P(P - 2)$  pyramids.

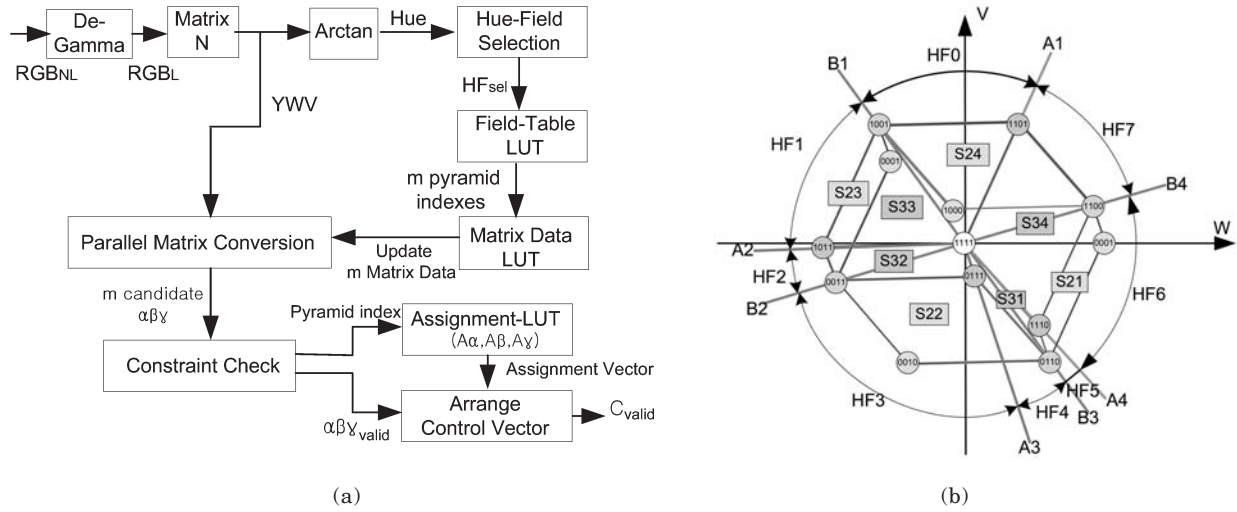


**Figure 5.** (a) Block diagram of the parallel matrix switching, and (b) example of individual hue field division (HF0~HF7) for 4 primary MPD: S21~S24 indicate the base planes of pyramids

As proposed by Ajito, the computation of a control vector for given  $\mathbf{F} = (X, Y, Z)^T$  tristimulus values is a solution to the following linear equation (see Fig. 3(b)):

$$\mathbf{F} = \alpha^* \mathbf{F}_1 + \beta^* (\mathbf{F}_2 - \mathbf{F}_1) + \gamma^* (\mathbf{F}_3 - \mathbf{F}_1), \quad (3)$$

where  $\mathbf{F}_i$  designates the tristimulus vectors for the control values  $\mathbf{C}$  in the circular nodes (Fig. 4(a)).

Equation (3) is slightly different from Ajito's method<sup>10</sup> in that it utilizes the independent scale factor  $\alpha$ , instead of  $v$ . In his method, he designed the scale factor  $v$  as a modulation factor of an unit vector  $U$  ( $U = \mathbf{F}_1 + \beta^* (\mathbf{F}_2 - \mathbf{F}_1) + \gamma^* (\mathbf{F}_3 - \mathbf{F}_1)$ ), and  $\mathbf{F} = vU$ , which has the same direction of the given vector  $\mathbf{F}$ . By modulating  $v$ , in the range of  $0 \leq v \leq 1$ , the modulated vector varies within the pyramid along the direction of the given vector  $\mathbf{F}$ . So, to find the solution, he solved the linear equation  $\mathbf{F} = vU$ .

The principal approach of our method is the same, but the computed scale factors ( $\alpha, \beta, \gamma$ ) are directly mapped to the control values. In addition, we can simplify not only physical constraint conditions of the control values but also existence condition of the given color vector  $\mathbf{F}$  within a pyramid directly from the three independent factors ( $\alpha, \beta, \gamma$ ).

In Eq. (3), the scale factors  $\alpha, \beta, \gamma$  are the final control values for an input color vector  $\mathbf{F}$ . First, its range has to fulfill the physical constraint condition  $0 \leq (\alpha, \beta, \gamma) \leq 1$ . To assign the solved  $(\alpha, \beta, \gamma)$  to the channel control values  $\mathbf{C} = (C_1, C_2, C_3, C_4)^T$ , we applied the exclusive-OR bit-operation between the control values of vertices of a selected pyramid. For example, the pyramid with the base plane of S32 and black point in Fig. 4(a) (as indicated in magenta) delivers three vertex control vectors of  $\mathbf{C}_{F1} = (0011)^T$ ,  $\mathbf{C}_{F2} = (1,0,1,1)^T$  and  $\mathbf{C}_{F3} = (0,1,1,1)^T$ . Through the bit-operation between  $\mathbf{C}_{F1}$  and  $\mathbf{C}_B = (0,0,0,0)^T$ , the assignment vector  $\mathbf{A}_\alpha = \mathbf{C}_{F1} - \mathbf{C}_B = (0,0,1,1)^T$  is delivered for  $\alpha$ . Multiplying  $\alpha$  with the result, we get the temporal result  $(0,0,\alpha,\alpha)^T$ . The same procedure should be applied for  $\beta$  (between  $\mathbf{C}_{F1}$  and  $\mathbf{C}_{F2}$ :  $\mathbf{A}_\beta = (1,0,0,0)^T$ ) and  $\gamma$  (between  $\mathbf{C}_{F1}$  and  $\mathbf{C}_{F3}$ :  $\mathbf{A}_\gamma = (0,1,0,0)^T$ ), then the final control vector  $\mathbf{C} = (\beta, \gamma, \alpha, \alpha)^T$  is obtained for this example.

In addition, the color vector  $\mathbf{F}_i$  in Eq. (3) is replaced by a linear transformed YWV signal instead of XYZ in our modified method:

$$\begin{pmatrix} Y \\ W \\ V \end{pmatrix} = T \cdot \begin{pmatrix} X \\ Y \\ Z \end{pmatrix}, \text{ with } T = \begin{pmatrix} 0 & 1 & 0 \\ -0.54 & -0.187 & 0.643 \\ 1.823 & -1.478 & -0.234 \end{pmatrix}. \quad (4)$$

According to the Rec. 709, Eq. (4) can be rewritten by the relationship ( $M_{709}$ ) between linear  $RGB_L$  and XYZ as follows:<sup>14</sup>

$$\begin{pmatrix} Y \\ W \\ V \end{pmatrix} = T \cdot M_{709} \begin{pmatrix} R_L \\ G_L \\ B_L \end{pmatrix} = N \cdot \begin{pmatrix} R_L \\ G_L \\ B_L \end{pmatrix} \text{ with } N = \begin{pmatrix} 0.213 & 0.715 & 0.072 \\ -0.25 & -0.249 & 0.5 \\ 0.433 & -0.433 & 0 \end{pmatrix}. \quad (5)$$

The main reason for using YWV space is to make an efficient ASIC design. Because YWV space has the similar construction as the well-known YCbCr space, we regard it as a linear YCbCr space (see Figs. 6 through 8). The transformation of the diagonal gray axis of the color gamut in XYZ into the Y-axis of the YWV coordinate system makes a gamut mapping in such YWV space more convenient than in the XYZ space because of the simple computation of chroma and hue H:

$$\text{Chroma} = \sqrt{W^2 + V^2} \text{ and } H = \text{Arctan} \left[ \frac{V}{W} \right]. \quad (6)$$

Moreover, the YWV space is more suitable for identifying candidate pyramids for parallel processing, and the unified signal flow in the whole process makes a simple ASIC design.

To find the appropriate pyramid for a given YWV input, a parallel process for the candidate pyramids has been developed, instead of the chromaticity LUT. The whole process is shown in Fig. 5(a). First, we get a linear  $RGB_L$  signal through out the de-gamma block according to the Rec.709 tone curve characteristic. Then, by the multiplying the matrix  $N$  (Eq. (5)) to the linear

**TABLE I. Hue Field Regions (HF0~HF7) and the Related Base Planes of Pyramids**

	S21	S22	S23	S24	S31	S32	S33	S34	Hue Range a	Hue Range B
HF0				○			○		A1~A2	~B1
HF1			○				○			B1~B2
HF2			○			○			A2~A3	
HF3		○				○				B2~B3
HF4		○			○				A3~A4	
HF5	○				○					B3~B4
HF6	○							○	A4~A1	
HF7				○				○		B4~

RGB<sub>L</sub> signal, we obtain YWV signal. This YWV signal is introduced into the parallel matrix block and the hue (Eq. (6)) of the signal is computed.

The second step is to find candidate pyramids for the computed hue. To do this, the WV-plane is intentionally divided into several hue fields by constant hue lines. Figure 5(b) is an example for a  $P = 4$  channel MPD case. On the diagram in Fig. 5(b), the parallelograms  $S_{ij}$  represent all base planes of the  $P(P - 2) = 8$  pyramids. These base planes can be divided into two subgroups as S21 ~ S24 and S31 ~ S34 (see Fig. 4(a)). As shown in Fig. 5(b), the base planes of each subgroup do not overlap each other in WV-color coordinates. But, there are overlaps of pyramids of the different subgroups. Hence, hue fields should be divided by the selection of the “Ai” hue lines (Fig. 5b) between the white point (1111) and 4 vertex points of the nodes (1110, 0111, 1011, 1101), see Fig. 4(a).

With this first hue division, we get the 4 related base planes within each hue field, see Table I, “HUE RANGE A”. More minimization can be done by applying the same method for the second subgroup S21~S24 (“Bi” hue lines in Fig. 5(b) and the corresponding “HUE RANGE B” in Table I). However, further hue division across the nodes of the primary colors (1000, 0100, 0010, 0001) does not minimize the number of related pyramids.

Generally, we get  $m = (P - 2)$  related pyramids in each hue fields by applying hue division with  $P(P - 2)$  hue lines or hue fields. For our 5 channel case, we get 3 related pyramids in each hue field with the 15 hue fields. So, we could reduce calculation of  $(\alpha, \beta, \gamma)$  from the 15 parallel processes to only  $m = 3$  parallel processes. It naturally reduces the computational complexity.

In Fig. 5(a), the parallel process was realized for every pixel signal by the hue field selection. The output signal  $HF_{sel}$  indicates an associated hue field (one of  $HF_i$ ), for an input signal. With the  $HF_{sel}$ , we find the related pyramid indexes as shown in Table I respectively.

The next step is then to update the  $M$  matrix data for the parallel matrix conversion block from the matrix data LUT, which has all coefficients of conversion matrixes (from YWV to  $\alpha\beta\gamma$  for all pyramids). Thereby, the required matrix coefficients are addressed by the  $HF_{sel}$ , more precisely its related pyramid indexes from Field Table LUT (see Table I). As a result of the parallel matrix conversion, we get  $m$  candidate control vectors  $(\alpha, \beta, \gamma)_1 \sim (\alpha, \beta, \gamma)_m$  for a given input YWV.

The following step is then the checking of the two constraint conditions. For these  $m$  candidate vectors, we check valid vectors by the already mentioned physical constraint  $0 \leq (\alpha, \beta, \gamma) \leq 1$ . Even if the physical constraint has been satisfied, more than one solution can be delivered during parallel processing for given candidate pyramids. Figure 3(c) indicates an example of this situation. The given vector  $F$  in the pyramid  $p1$  can be recon-

structed by a linear combination of two different vectors ( $F_{p1}, F_{p2}$ ) in the pyramids  $p1, p2$ .

To obtain the best solution, or to ensure the contourless image rendering, the continuity of control values for given continuous tristimulus values is required. To meet this goal, additional conditions should be necessary. The required condition was taken from a trigonometrical proportionality term as shown in Fig. 3(d). For the triangle ( $B, F1, F2$ ), we can formulate the proportionality equation as  $F1/(F2 - F1) = v\alpha * F1/L_{max}$ . The existence of the component vector  $\beta * (F2 - F1)$  within the pyramid will be satisfied, if  $\beta * (F2 - F1)$  is smaller than  $L_{max}$ . It results in the additional conditions of  $\alpha \geq \beta$ , and  $\alpha \geq \gamma$  for the other  $\gamma * (F3 - F1)$  component vector analogously. With these conditions, we always get a best single solution for any given vector  $F$ .

At the same time, we know which pyramid was selected for the valid vector  $(\alpha, \beta, \gamma)_{valid}$ . With this pyramid index, we take the previously mentioned assignment vectors ( $A\alpha, A\beta, A\gamma$ ) out of the Assignment-LUT in Fig. 5(a). Under consideration of ( $A\alpha, A\beta, A\gamma$ ), the final valid vector  $(\alpha, \beta, \gamma)_{valid}$  should be arranged into the appropriate channels.

In this section, we explained about the modified matrix switching. The main difference of our method in comparison with Ajito’s method is the parallel processing using hue decision in order to find an appropriate control vector, e.g., pyramids, instead of a 2D chromaticity LUT, and the use of YWV signal instead of XYZ for an efficient ASIC design.

### Gamut Matching

In the conventional television industry, there are two kinds of color reproduction methods. The first one is colorimetric reproduction which tries to reproduce exactly same colors of originals in the broadcast. The other one is preferred color reproduction. In this case, television-viewer does not know the original colors so that the television maker tries to enhance the picture quality using scene adaptive image enhancement algorithms, such as contrast and color saturation enhancement. In such a case, a judgment of picture quality is very subjective and difficult. Gamut mapping is one of the preferred color reproduction methods. Therefore, it is not simple to evaluate the picture quality. In this aspect, our study on gamut mapping may imply the need for more effort and time on picture quality evaluation in future. Hence, in this article, we focus only on the mapping concept and developing efficient algorithms

To utilize the full range of the MPD color gamut for the input Rec. 709 signal, two kinds of gamut matching methods have been developed. The first method is gamut mapping in an intensity linear YWV color space. This mapping strategy has an advantage in a relative simpler hardware implementation. In contrast, a second

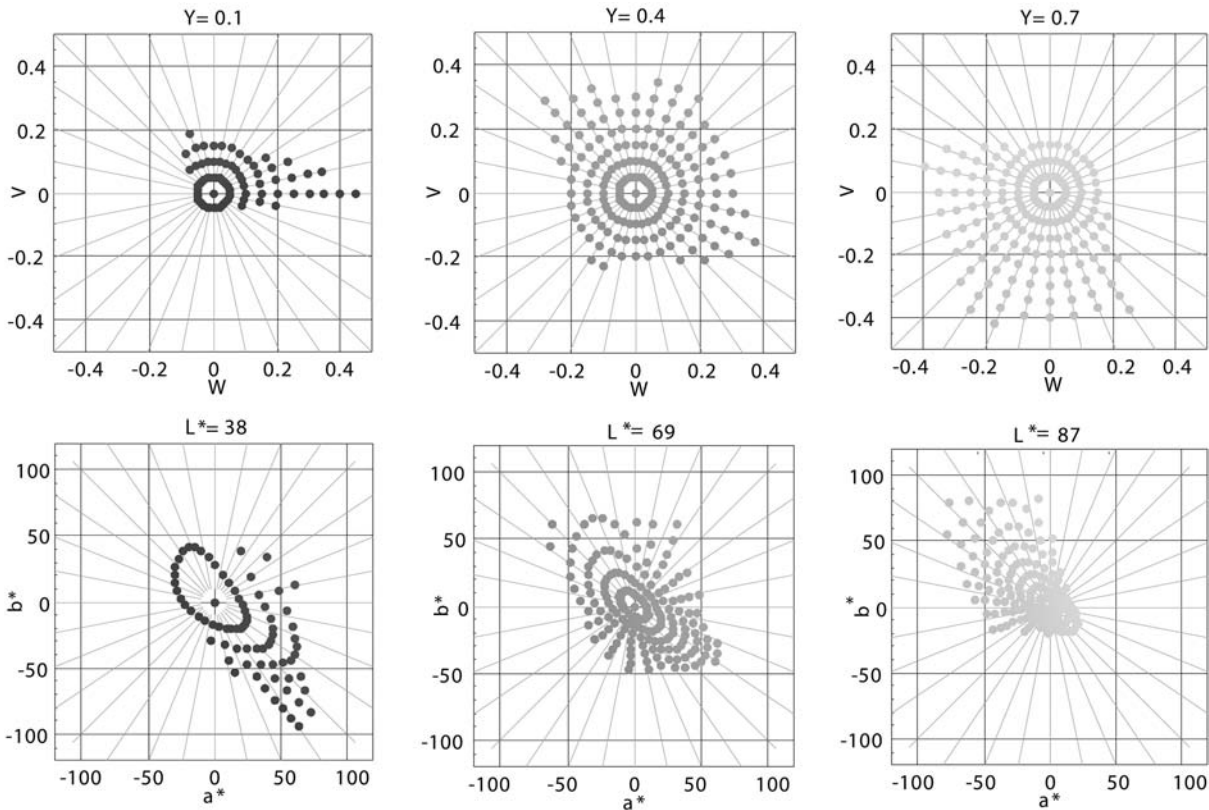


**Figure 6.** Upper: equally quantized colors on  $Y = \text{constant}$  WV-planes with equidistant hue ( $11.25^\circ$  step) and chroma (0.05 step), Lower: their transform into CIE- $L^*a^*b^*$ .

mapping method is carried out in a uniform color space. This is a common concept in color science and generally delivers a better result. However, it is very time costly due to complex transformation and determination of gamut boundaries. For real time processing, it often needs a large amount of memory. Therefore, our study has investigated in both methods.

For the first method, we transformed the XYZ color gamut in YWV color space. And, the chroma axes (W,V) are roughly rescaled uniformly according to human perception so that the required processing bit depth of the YWV signal is less than for the tristimulus signal XYZ.<sup>13</sup> Typically, we needed 12 bits/channel in our FPGA implementation for the proper quantization of MPD color gamut.

Figure 6 shows the characteristic of constancy and uniformity of hue and chroma in comparison with transformed CIE- $L^*a^*b^*$  color values. The upper three  $Y = \text{constant}$  planes show the colors which are equally quantized for equidistant hue and chroma values in YWV space, and the lower three plots indicate the transformed colors on CIE- $L^*a^*b^*$  space. As shown in Fig. 6, generally, the hue- and chroma-uniformity of the linear YWV color space is not sufficient. However, one of the important characteristics during the gamut mapping is hue constancy.

Figure 7 shows six color scales, which are equidistantly quantized in the direction of chroma at constant hue and luminance/lightness in each YWV and CIE-LAB color space. As shown in Fig. 7, a judgment of the hue constancy in both spaces is quite difficult, but the visual hue constancy of YWV is much better in the blue-

purple region where the hue constancy in CIE- $L^*a^*b^*$  space is not satisfactory.

Figure 8 shows the gamut of the Rec. 709 in comparison with the gamut of the MPD for the constant hue and shows the concept of the gamut mapping in that space. As shown in the figure, MPD has generally more volume of gamut than the Rec. 709 space. However, as mentioned before, RGB primary colors of Rec. 709 have higher luminance than the colors of MPD with the same chromaticity. Therefore, the gamut mapping in such color regions requires more effort. The simplest way of gamut matching will be chroma matching at a constant lightness and hue, as shown in Fig. 8 (brown line). In most cases, this chroma mapping operates quite well. However, in the gamut compression case, the method has a desaturation effect in the color region of RGB primary colors of Rec. 709, and this degradation of the red color may be perceptually worse than of the other primary colors.

Instead of chroma matching, an alternative vector mapping (plotted as the blue line) can be applied to reduce the desaturation effect. It only changes magnitudes of the color vectors at the same chromaticity coordinates. But in some situations, this method has also another problem of a large transition of luminance levels in or near the cross point of two gamut boundaries (marked as a gray circle in Fig. 8). It may cause a contouring problem in the image rendering.

More sophisticated, adaptive vector-chroma mapping can be also applied (as marked in magenta). Thereby, the mapping angle  $\vartheta$  may be varied as a function of the luminance, so that the above mentioned desaturation



**Figure 7.** Hue constancy of YWV in comparison with CIE-LAB (all color scales are quantized by 10 equidistant chroma at constant hue and luminance/ lightness): Hue deviation in blue and red color scale of CIELAB can be observed.

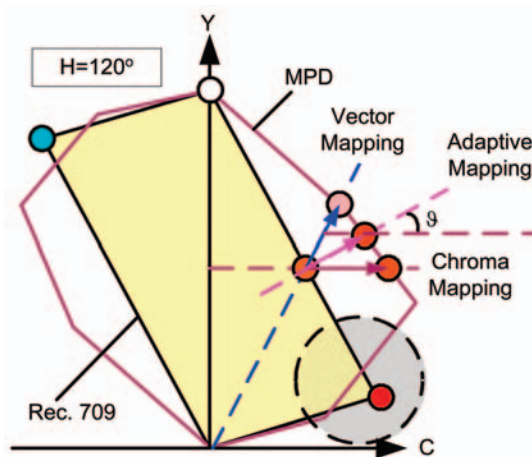


**Figure 8.** Gamut comparison in YWV space and mapping concept.

and the contouring problem will be effectively minimized. This method may be more complex and will be our future work.

The relative simpler implementation of gamut mapping in intensity linear color space (YWV) sometimes needs a careful optimization process. In fact, YWV space is not a uniform space so that applying linear compression or stretching of the chroma or color vector leads to visually nonuniform alteration of chroma and luminance. In our experiment, we had that problem in the strongly expanded color region of the MPD gamut in relation to Rec.709, especially in cyan and orange regions (Figs. 10(a) and 10(b)). Some mapped images, which include such colors, result in an unnatural impact. To prevent this phenomenon, a limitation of stretching gain or nonlinear compression (such as a cube root function) should be applied in these color regions. Hence, further investigation was carried out in a uniform color space.

Recently, many of uniform color spaces are available. Fig. 9 shows the gamut comparison in a uniform color

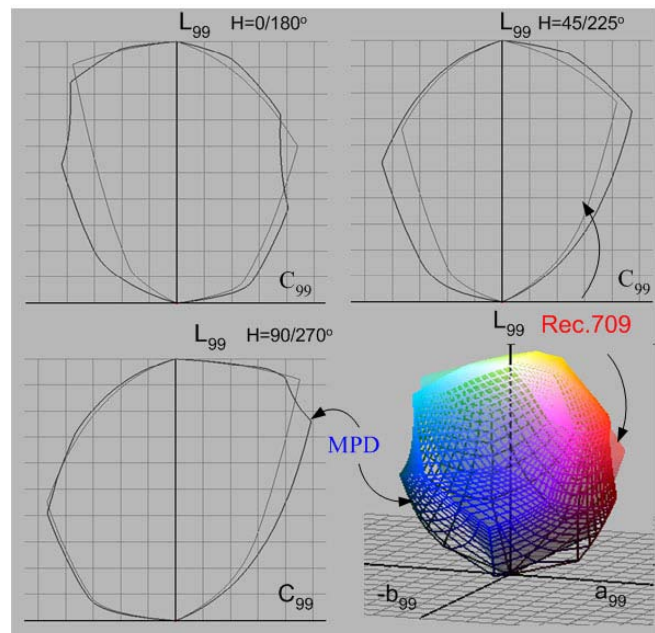


**Figure 9.** Gamut comparison in uniform DIN99d color space:  $L^*C^*$  cuts for variety hues, thin line indicates Rec. 709 and thick line indicates MPD gamut boundaries and perspective view of 3D gamut (frame for MPD, volume for Rec. 709 gamut).

space based on the DIN99d color difference formula.<sup>15</sup> Below, this color space will be referred to as being the  $LAB_{99d}$  space. The chosen  $LAB_{99d}$  was constructed mainly by two modifications in regard to CIELAB<sub>76</sub>: the logarithmic transformation of lightness and the logarithmic chroma compression in radial direction with reduced blue-yellow weighting. Consequently, the uniformity of color difference was quite improved over the whole gamut. In such an improved uniform color space, we

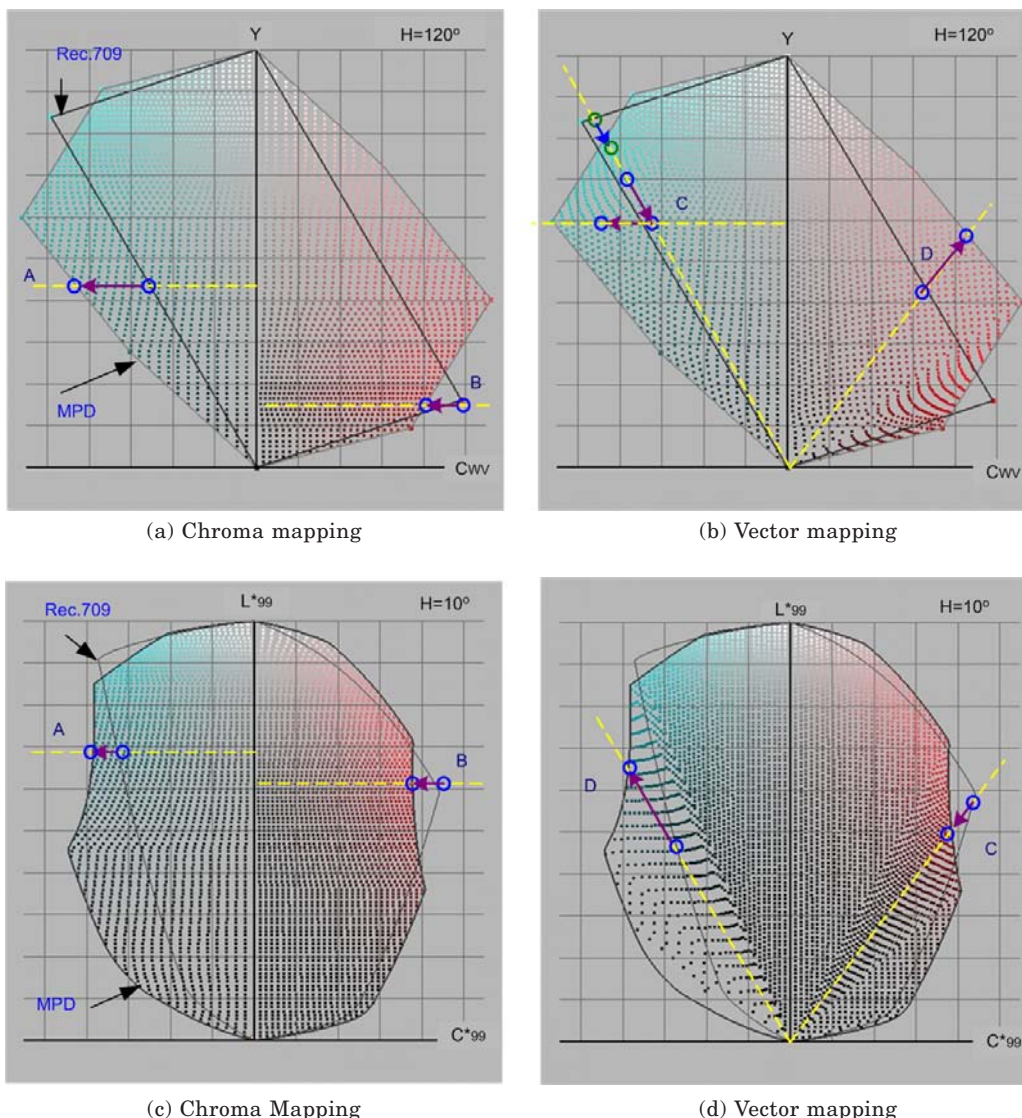


**Figure 10.** Gamut mapping results; (a), (b): mapping in YWV space (c), (d): mapping in LAB<sub>99d</sub> Space. A: chroma stretching, B: chroma compression, C: adaptive mapping (vector compression + chroma stretching), and D: vector stretching.

could apply the same chroma or vector mapping concepts much more effectively and conveniently. Therefore, it delivers a better natural image reproduction than YWV space with the same algorithm concepts and requires a shorter optimization process. Figures 10(a) through 10(d) shows typical mapping results in YWV and LAB<sub>99d</sub> color space. The equally spaced colors within the Rec. 709 gamuts in YWV and LAB<sub>99d</sub> matched to the MPD color gamuts according to these chroma and vector mapping methods.

The chroma stretching (Fig. 10(a), A) in YWV enlarges the chroma in cyan colors too much, which sometimes causes unnatural images. Furthermore, the red color of Rec709 will be desaturated as shown in Fig. 10(a), B). For the full use of the expanded color gamut of MPD, color vector compression and successive chroma stretching are applied (Fig. 10(b), C). This combination method gives more natural results than the chroma stretching alone. If needed, an excessive gain of the chroma stretching will be limited for a more natural look. The compression of the vector mapping in the

red color region (Fig. 10(b)) prevents desaturation of those colors. However, it also causes a luminance attenuation problem.

The same mapping concept is applied to the color gamuts in LAB<sub>99d</sub>. In this case, we observed very similar results in reproduced images except for more uniform scaling in stretching and compression in contrast to the cases in YWV. Figure 10(d) shows the results of vector mapping. In this case, we do not need to combine chroma mapping as in Fig. 10(b), C). Because of the different shape of the color gamuts obtained by nonlinear transformation to LAB<sub>99d</sub>, only vector mapping can match most of the MPD gamut region. An excessive stretching gain in the cyan color region (Fig. 10(d), C) may produce a quantization error and boost the color noise of images as in the mapping in YWV space. The limitation of stretching gain may be required in practice. The main advantage of the mapping in LAB<sub>99d</sub> space is that we can estimate an appropriate stretching gain better than in YWV because of the uniform characteristics of the space.

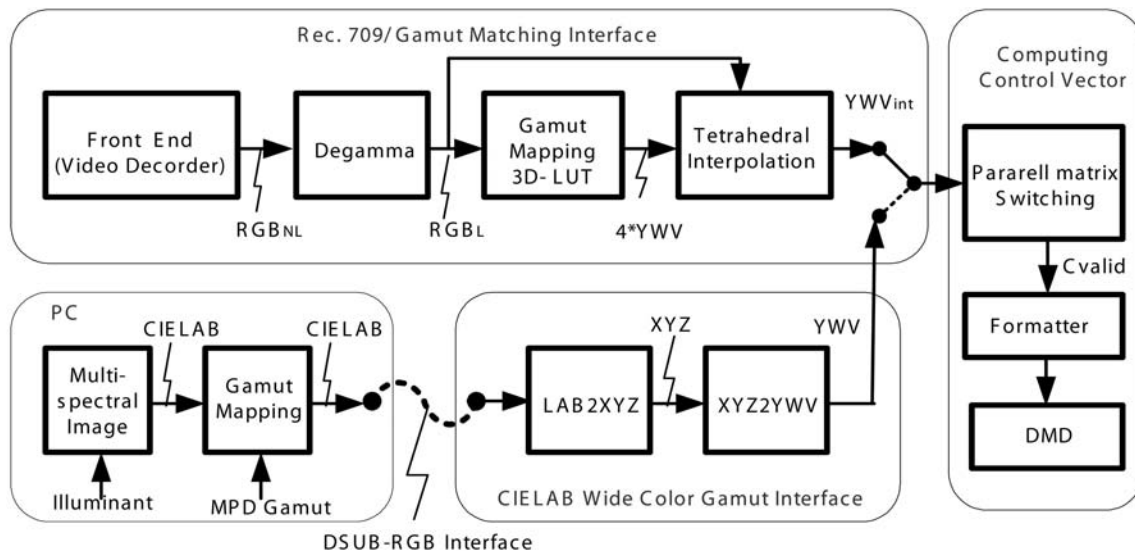


**Figure 11.** Simplified signal flow in FPGA.

### Implementation

The signal transformation into  $LAB_{99d}$  color space and the determination of the gamut boundaries are very complex and computationally intensive. Therefore, for real time processing, gamut mapping had been applied to the  $32 \times 32 \times 32$  equidistant linear  $RGB_L$  signals of Rec. 709 which should be obtained by inverse gamma from the non-linear  $RGB_{NL}$  of Rec.709. The corresponding  $Y_WV$  values for  $32 \times 32 \times 32$  lattice points were calculated using PC-based mathematical program and implemented as a color transformation table, as shown as a 3D-LUT in Fig. 11. Additionally, the 3D-LUT data can be final control values instead of  $Y_WV$  values. However, in order to share the parallel processing block with the CIELAB interface (lower block) it was purposely separated.

The next interpolation block then tries to compute the intermediate  $Y_WV$  values for given input  $RGB_L$  values by the conventional tetrahedral interpolation.<sup>16</sup> For this interpolation we need four  $Y_WV$  values as lattice points of a selected tetrahedron, in which a corresponding  $Y_WV$  for given  $RGB_L$  should be included. So, the interpolated values ( $Y_WV_{int}$ ) are delivered to the next control vector calculator.

The followed simplified parallel matrix switching block indicates the all functions of Fig. 5(a), detailed above. Throughout the parallel matrix switching block we obtain a valid control vector  $C_{valid}$  for the  $Y_WV_{int}$  signal. Then, the final control values are available for a formatter, in which the linear control values are specially prepared for the control of DMD™ (Digital Micro-mirror Device).

Contrary to the gamut matching method, we also implemented a  $CIELAB_{76}$  signal interface in order to test the rendering of wide gamut images. It is realized by using the conventional television RGB interface (DSUB-RGB) in a PC mode, so wide color gamut images in  $CIELAB_{76}$  format can be also reproduced.

For this experiment we used multispectral image data (MUSP) from Color Aixpert.<sup>17</sup> Firstly, we calculate CIELAB images for a given D65 illuminant of the viewing booth. Then, a necessary gamut mapping of not reproducible colors, which lie outside the MPD color gamut, is done by an external program on the PC before putting the signal into the interface. The driven

CIELAB signal via D-SUB interface is then converted into corresponding XYZ and  $Y_WV$  successively. The processing after this stage is common. All procedures are shown in the lower block diagram of Fig. 11.

Finally, the FPGA board allows two kinds of image reproduction for the wide gamut signal in CIELAB via conventional PC-RGB interface ( $8 \times 3$  bits resolution) and for the limited color gamut of Rec. 709 with the gamut matching algorithm for HDTV application. The display allows reproduction of the progressive video stream with a pixel resolution of up to  $1280 \times 720$  at the contrast ratio of 1000:1 and the white luminance of about  $400 \text{ cd/m}^2$ .

### Experiments

Above, we discussed the computing of control values for given intensity linear  $Y_WV$  (or tristimulus XYZ) values. After color patch measurement, the average color reproduction error recorded was  $\Delta E_{ab} = 2.35$ , with a maximum  $\Delta E_{ab} = 5.8$  for the measurements of 243 ( $3 \times 3 \times 3$ ) color patches, for which XYZ values are computed from all the combinations of linear control values with (32, 128, 255 in 8 bit resolution) levels for each channel. It assures an accurate colorimetric reproduction on the MPD screen.

For a test of real life images, wide gamut images with natural and artificial objects were captured using the commercially available multispectral camera system for Color Aixpert in Germany.<sup>17</sup> Their spectral data were converted into CIELAB values for a D65 simulator lamp in the viewing booth (Minolta GTI Color Matcher), and the reproduced images on the screen were compared with the originals in the viewing booth. Within the gamut of reproducible colors, the MPD provides much more vibrant colors than the conventional CRT display and therefore more color details are visible. Figure 12 shows this simulation result. More colors of the two original (top) MUSP images can be reproduced on MPD (mid) than on CRT (bottom); not reproducible colors are marked as black.

The other approach of this study was to develop a gamut matching method to use the full range of color gamut of MPD for given signal with limited color gamut. To infer the suitability of the matching algorithms for

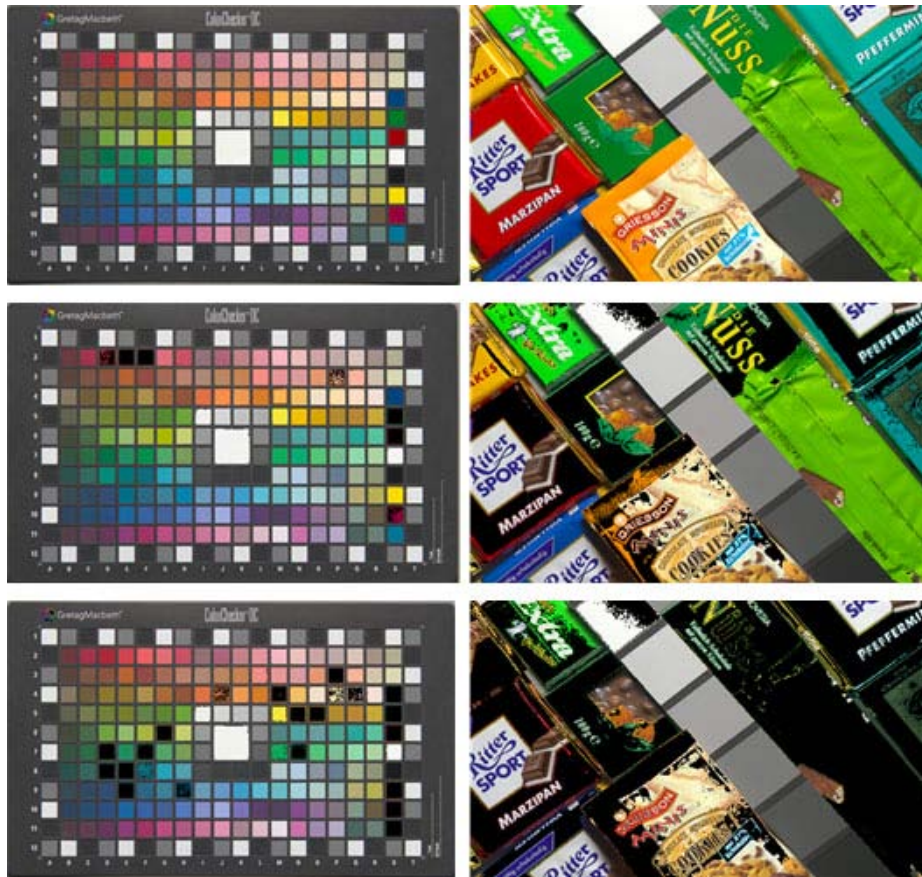


**Figure 12.** Original MUSP images (Top), reproduced images on MPD (Mid), and reproduced on CRT (Bottom); black-marked pixels are colors out of each display gamut.

consumer television, with respect to color saturation enhancement for wide gamut MPD, until the establishment of the future wide color gamut broadcasting signals two kinds of mapping algorithms have been applied to Rec. 709 video pictures. Generally, the gamut matching in  $LAB_{99d}$  provides a better result than in YWV space in terms of a natural look of reproduced images due to the uniform scaling of the color space under the same mapping concepts. The careful optimization of the mapping parameters in YWV domain, such as nonlinear stretching/compression gain, limitation of excessive stretching gain in some color regions, and hue-adaptive gain, also indicates almost the same reproduction result as in  $LAB_{99d}$ .

The mapping in YWV needs more development time on the one hand, but it allows the real time processing with relatively small hardware resources on the other hand. Contrary to that, the optimization process of the mapping in  $LAB_{99d}$  is much more robust due to the uniform color space. The choice of the mapping algorithm is mainly dependent upon its application.

We also observe that a visual impact of the reproduced images varies by the mapping methods and adjustment of the adaptive mapping angle  $\vartheta$  in Fig. 8. If the mapping line assigned lies near the vector mapping line, then the reproduced images are more natural. One of the reasons is that modulation of the color vector can be interpreted as due to the same effect; i.e., color outcome under the intensity variation of an illuminator. So, to find an optimal mapping angle is one of many

important issues in application of such an algorithm and it is the direction of our future work. On the other hand, the near-chroma mapping line (especially in a stretching situation) yields more vibrant images as a result of the relative increase of chroma compared to lightness of color vectors.

Altogether, the relative increase of chroma and lightness by gamut mapping creates an increase in perceived brightness and colorfulness in comparison to conventional systems. It may result in improved color contrast and sharpness. It delivers a much higher visual impact for reproduced pictures.

### Conclusion

The focus of this article is to describe a method that allows using a full range of color gamut of MPDs for a given limited color gamut signal of the current television system so that the limited color saturations are adaptively expanded. The study also treated further issues of related gamut mapping concepts and their practical implementation, especially for application to real time processing. Thanks to the wider color gamut and the appropriate gamut matching algorithm, the picture quality of MPD is significantly improved. The system was implemented in FPGA and it enables motion picture reproduction up to HD format size in real time. For better picture quality, our research is still directed towards an advanced gamut matching method and a new system configuration such as a four-primary display and a new illumination system, in order to compensate for

the lower luminance of RGB primary colors. In this study, we could not fully emphasize image quality from the viewpoint of human perception which should be assessed further. In addition, the modified matrix switching is weak with respect to noise immunity in the dark colors. One of our next challenges is to develop a robust and simple inverse display model.

**Acknowledgment.** The author gratefully thanks Prof. B. Hill and Dr. Herzog at Aachen University of Technology and at Color Aixpert GmbH for many helpful discussions and advice, and also Mr. H. Bellis at Texas Instruments Inc. U.S. and Mr. S. Koichi at Samsung for cooperation in FPGA implementation.

## References

1. M. R. Pointer, "The gamut of real surface colours", *Color Res. Appl.*, **5**, 145–155 (1980).
2. ITU-R.BT.1361, Worldwide unified colorimetry and related characteristics of future television and imaging systems.
3. IEC61966-2-2, Extended RGB colour space – scRGB.
4. G. Hollemann, "High power laser projection displays", *Proc. SPIE*, **4294**, 36–46 (2001).
5. M. C. Kim, S. H. Dho and I. Moon, "Colorimetric aspect and development status of RGB laser displays", *CLEO-Europe 2003 Conference*, (SPIE Press, Bellingham, WA, 2003), Tech-Focus Topics, TFI.
6. H. Suigiura, "Wide color gamut monitors: LED Backlighting and new phosphor CRT", *Proc. SPIE*, **5289**, (2004).
7. I. Childs and A. Roberts, "Decoding colour video signals for display", UK Patent 2282928 (1995).
8. B. Hill, "(R)evolution of color imaging systems", *Proc. 1st European Conference on Color in Graphics, Imaging and Vision CGIV 2002*, (IS&T, Springfield, VA, 2002), pp. 473–479.
9. F. Koenig, K. Ohsawa, M. Yamaguchi, N. Ohayama, and B. Hill, "A Multi-Primary Display: Optimized Control Values for Displaying Tristimulus Values", *Proc. IS&T's PICS Conference*, (IS&T, Springfield, VA, 2002), pp. 215–220.
10. T. Ajito, "Color conversion method for multiprimary display using matrix switching", *Opt. Rev.* **8**, 191–197 (2001).
11. H. Motomura, Backward model for multi-primary display using linear interpolation on equiluminance plane, *Proc. IS&T/SID 10<sup>th</sup> Color Imaging Conf.*, (IS&T, Springfield, VA, 2002), pp. 267–271.
12. M. Yamaguchi, "Color image reproduction based on the multispectral and multiprimary imaging: Experimental evaluation", *Proc. SPIE*, **4663**, 15–26 (2002).
13. B. Hill, "Comparative analysis of the quantization of color spaces on the basis of the CIELAB color difference formulae", *ACM Trans. Graphics*, **16**, 109–154 (1997).
14. ITU-R.BT.709-4, Parameter values for the HDTV standards for production and international program exchange.
15. G. Cui, M. R. Luo, B. Rigg, G. Roesler, and K. Witt, "Uniform colour spaces based on the DIN99 colour difference formula", *Color Res. Appl.* **27**, 282–290 (2002).
16. Henry R. Kang, "Comparisons of Three-dimensional Interpolation Techniques by Simulation", *Proc. SPIE* **2414**, 104–114 (1995).
17. www.color-aixperts.de
18. J. Morovic and M. R. Luo, "The Fundamentals of Gamut Mapping: A Survey", *J. Imaging Sci. Technol.* **45**, 283–290 (2001).